Chemical reactivity between sol–gel deposited Pb(Zr,Ti)O_3 layers and their GaAs substrates

Benjamin Meunier, Ludovic Largeau, Philippe Regreny, Jose Penuelas, Romain Bachelet, Bertrand Vilquin, Baba Wague, Guillaume Saint-Girons

▶ **To cite this version:**

Benjamin Meunier, Ludovic Largeau, Philippe Regreny, Jose Penuelas, Romain Bachelet, et al.. Chemical reactivity between sol–gel deposited Pb(Zr,Ti)O_3 layers and their GaAs substrates. CrystEngComm, 2016, 18 (39), pp.7494. 10.1039/C6CE01276K . hal-01489114

HAL Id: hal-01489114
https://hal.science/hal-01489114

Submitted on 28 May 2024

HAL is a multi-disciplinary open access archive for the deposit and dissemination of scientific research documents, whether they are published or not. The documents may come from teaching and research institutions in France or abroad, or from public or private research centers.

L'archive ouverte pluridisciplinaire **HAL**, est destinée au dépôt et à la diffusion de documents scientifiques de niveau recherche, publiés ou non, émanant des établissements d'enseignement et de recherche français ou étrangers, des laboratoires publics ou privés.

Chemical reactivity between sol–gel deposited PbIJZr,Ti)O_3 layers and their GaAs substrates

B. Meunier,[a] L. Largeau,[b] P. Regreny,[a] J. Penuelas,[a] R. Bachelet,[a] B. Vilquin,[a] B. Wague[a] and G. Saint-Girons[a]

We show how chemical interactions between the growing material and the substrate affect the crystalliza-tion of PbIJZr,Ti)O3 (PZT) thin films on SrTiO3-templated GaAs substrates. A liquid PZT precursor (sol) is spin-coated on STO/GaAs pseudo-substrates grown by molecular beam epitaxy and crystallized by annealing under air. Complete crystallization of the PZT layers cannot be achieved due to significant oxida-tion of the GaAs substrate which enhances As diffusion through the structure and further formation of par-asitic compounds containing Pb, Sr and As due to the strong chemical affinity between As anions and Pb and Sr cations. These mechanisms are extensively studied based on X-ray diffraction measurements carried out in situ during annealing and on transmission electron microscopy experiments including energy-dispersive X-ray analyses.

Introduction

In the past few decades, microelectronic processes have mostly been powered by constant miniaturization of Si/SiO_2 based devices. This purely Si-based strategy has for several years been identified as a dead-end, due to intrinsic limitations of the Si/SiO_2 system. Diversification and integration of materials and concepts used in microelectronic processes (so-called "More than Moore strategy") is now unanimously considered as a key issue for the development of micro-optoelectronics.[1] Future chips will combine more and more functions for RF connectivity, built-in sensors, data storage, photonic circuits, *etc.* In this context, the combination on the same wafer of materials having different physical properties is a key challenge. Amongst the materials of interest, III–V semiconductors, which can be combined by epitaxy, are the object of specific attention because their optoelectronic and transport properties are superior to those of silicon. Similarly, so-called functional oxides, especially those having a perovskite structure, have unique physical properties (ferroelectricity, ferromagnetism, piezoelectricity, *etc.*) that make them very attractive for various applications in microelectronics, spintronics, biophysics, MEMS, energy harvesting, *etc.*[2] One of the main advantages of these oxides is that most of them can be also combined with each other by epitaxy to form multifunctional heterostructures. Beyond the integration strategy of functional oxides into microelectronic platforms, the combination of functional oxides and semiconductor properties by epitaxy would lead to a new class of integrated optoelectronic devices. The pioneering studies of McKee *et al.* have opened a path toward the realization of functional heterostructures combining oxides and semiconductors by showing that $SrTiO_3$ (STO) can be directly grown on silicon by molecular beam epitaxy (MBE) to fabricate STO/Si pseudo-substrates.[3,4] Using such pseudo-substrates, various functional oxides have been integrated into Si wafers, such as $Sr_xBa_{1-x}TiO_3$,[5] $BaTiO_3$ (BTO)[6–9] and PMN-PT.[10] Following the same strategy, MBE growth of STO on GaAs has been demonstrated[11] as well as integration of ferroelectric BTO into such templates.[12,13] Amongst the oxides that can be integrated into STO templates, $Pb(Zr,Ti)O_3$ (PZT) is of particular interest because of its high remanent polarization (P_r), its low coercive field (E_c) and its outstanding piezoelectric properties.[14] Single-crystal ferroelectric PZT thin films were first integrated into STO/GaAs templates in 2013 using pulsed laser deposition (PLD),[15] and into STO/Si templates by sol–gel deposition,[16–19] as the sol–gel process offers a cheaper and simpler alternative to other oxide deposition techniques such as PLD or sputtering. More recently, integration of ferroelectric PZT on GaAs using the sol–gel process has been described, reporting a degradation of the sample surface attributed to the presumed interdiffusion mechanism between PZT and GaAs.[20]

Here, we report a detailed study of the chemical interactions between PZT and STO-templated GaAs during the sol–gel growth of the piezoelectric oxide. This study is based on *in situ* X-ray diffraction experiments carried out during

[a] *INL-UMR5270/CNRS Ecole Centrale de Lyon, Université de Lyon, 36 avenue Guy de Collongue, FR-69134 Ecully cedex, France.*
E-mail: benjamin.meunier@ec-lyon.fr
[b] *Laboratoire de Photonique et de Nanostructures (LPN), CNRS, Université Paris-Saclay, Route de Nozay, 91460 Marcoussis, France*

sample annealing, and structural and chemical studies performed using scanning transmission electron microscopy (STEM) combined with energy dispersive X-ray spectroscopy (EDX).

Experimental

The samples considered in the following discussion were grown on (001)-oriented GaAs substrates. A 500 nm GaAs buffer was first grown using a III–V dedicated MBE reactor, followed by room-temperature deposition of an As capping layer aimed at protecting the sample surface during its transfer under air to the oxide dedicated reactor. After sample introduction in the oxide-MBE chamber, this protective As capping layer was desorbed by heating the sample under ultra-high vacuum (UHV) up to 500 °C, leading to the formation of a (2 × 4) reconstructed As-terminated surface. The procedure extensively described in ref. 15, 21 and 22 was then used to grow 10 nm thick single-crystal STO layers. Previous studies have shown that at this step, the STO/GaAs interface is abrupt and in particular that oxygen has not diffused toward the GaAs substrate.[15] Spin-coating was then employed to spread a PZT 52/48 precursor solution from Mitsubishi Materials Corp. on the STO/GaAs templates. The samples were then calcined at 350 °C under air for 5 minutes to dry the sol film, leading to a smooth surface without hillocks. After these operations, a 33 nm-thick amorphous PZT was obtained. The process was then repeated in order to reach a PZT thickness of ~100 nm. Samples A, B and C were then annealed under air at 405, 420 and 510 °C, respectively, for 2 min to crystallize the PZT layer. A fourth sample was introduced into a Rigaku Smartlab diffractometer equipped with a rotating anode and a heating stage to monitor PZT crystallization by X-ray diffraction (XRD) during annealing under air. The temperature was gradually increased (ramp: 10 °C min^{-1}) from room temperature up to 520 °C. Every 10 °C, the sample was realigned and radial scans around the GaAs (004), STO (002) and PZT (002) reflections were recorded. Samples A, B and C were also characterized by XRD, STEM and EDX. A broad range XRD diffractogram recorded on sample B (annealed at 420 °C) is displayed in Fig. 1(a).

Whilst dominated by (00*l*) PZT reflections, this diffractogram also presents clear signatures arising from other PZT orientations, showing that at least part of the PZT

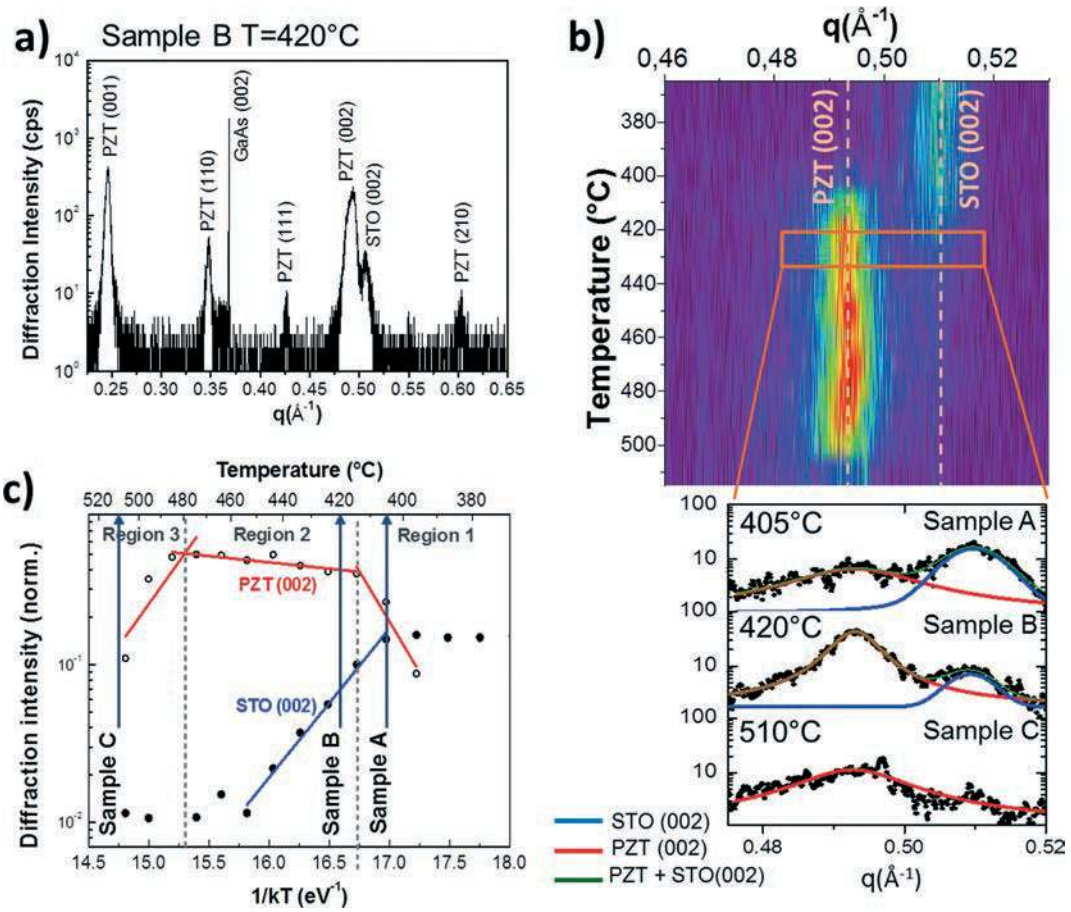

Fig. 1 a) Wide range XRD radial scan recorded on sample B (partially crystallized, annealed at 420 °C). *q* is the magnitude of the out-of-plane diffraction vector ($q = 1/d$ where *d* is the interatomic distance). b) XRD radial scans of the STO (002) and PZT (002) reflections recorded *in situ* during annealing and examples of resolution of a scan line. c) Evolution of the diffraction intensity, as recorded during *in situ* annealing (Arrhenius plot representation: *t* is the temperature and *k* the Boltzmann constant).

film is polycrystalline. The diffractograms shown in Fig. 1(b) were recorded during *in situ* annealing. They show the evolution of the STO (002) and PZT (002) reflections with annealing temperature. The intensity of the corresponding peaks is plotted as a function of the temperature in Fig. 1(c). Three regimes can be defined for the PZT (002) reflection: below 415 °C (region 1), the intensity of the STO (002) peak remains constant whilst that of the PZT (002) peak increases, indicating progressive PZT crystallization. Between 415 and 485 °C (region 2), the intensity of the PZT reflection continues to increase with a lower slope, while that of the STO reflection decreases due to degradation of the STO template. Further increase of the annealing temperature above 485 °C (regime 3) leads to rapid degradation of the PZT layer, as indicated by the decrease of the PZT reflection intensity.

Activation energies for the different processes can be extracted from Fig. 1(c): 280 kJ mol^{-1} for PZT crystallization in regime 1, 210 kJ mol^{-1} and 370 kJ mol^{-1} for STO and PZT degradation in regimes 2 and 3, respectively. The activation energy recorded in regime 1 is of the same order of magnitude as those reported for crystallization of sol–gel PZT layers deposited on various substrates,[23,24] confirming that the observed evolution corresponds to PZT crystallization. The other values will be discussed in the following section.

TEM and EDX characterization

In order to analyze the internal structure of the sample, we have used a 200 keV FEI Titan Themis TEM-STEM equipped with a probe aberration corrector and a super X Bruker silicon drift detector with an effective large angle of detection (0.98 steradian).

High angle annular dark field (HAADF)-STEM cross-sectional views of samples A, B and C are displayed in Fig. 2. The STO/GaAs and PZT/STO interfaces appear clearly in the image of sample A, attesting to the overall epitaxial quality of the heterostructure, with a cube-on-cube epitaxial relationship between the two perovskites and a 45° rotation between STO and GaAs. However, a darker region is clearly detected beneath the STO/GaAs interface, extending in the GaAs substrate to about 20 nm. This region corresponds to oxidized GaAs, as confirmed in the following discussion. As such substrate oxidation is not observed after STO growth by MBE,[20] it is caused by PZT deposition due to oxygen diffusion through the oxide stack towards the GaAs substrate. The

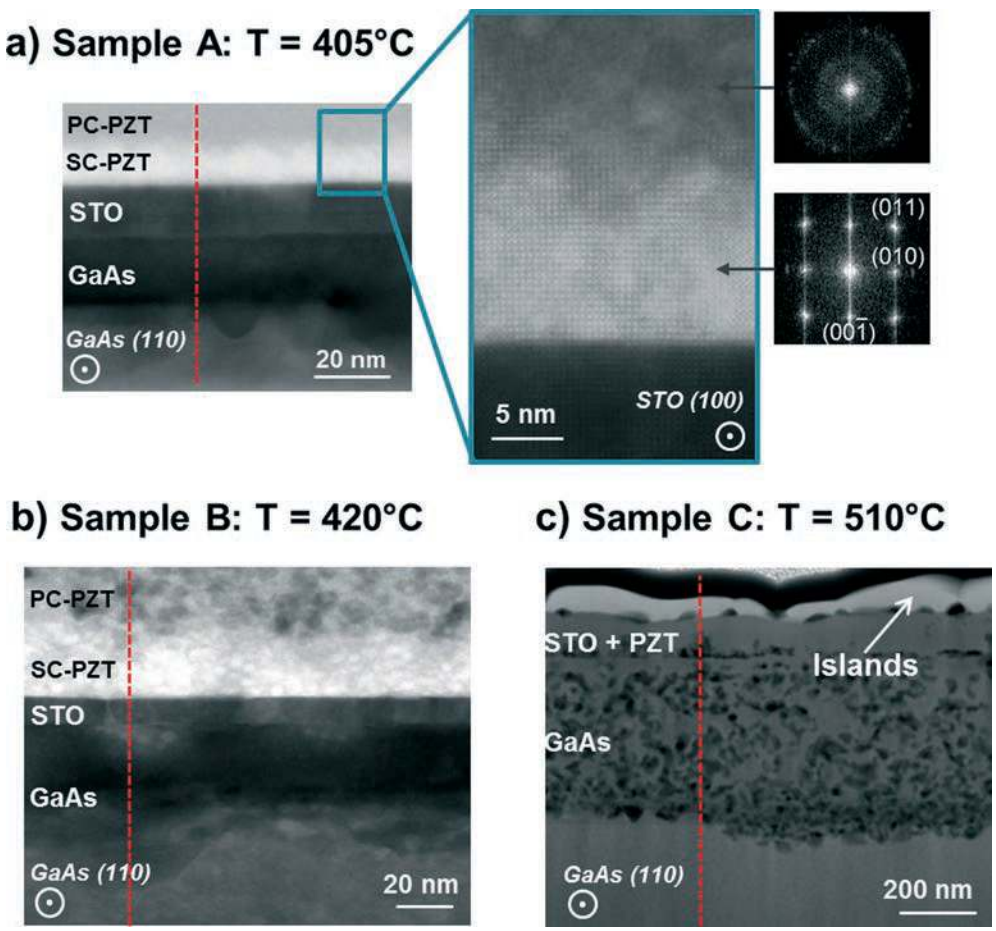

Fig. 2 HAADF-STEM cross-sectional views of samples A, B and C. Red dashed lines are those along which the EDX profiles displayed in Fig. 4 have been recorded.

zoomed view provided in Fig. 2(a) shows that the PZT layer is actually composed of a 10 nm thick single-crystal region near the PZT/STO interface (organized spots on the FFT), topped by a region composed of a mixture of amorphous PZT and small, randomly oriented PZT grains (rings on the FFT) where PZT crystallization is uncompleted. This observation is in good agreement with the XRD pattern displayed in Fig. 1(a). Interestingly, this single-crystal to amorphous/polycrystal transition is correlated to a change of the HAADF contrast, suggesting that the PZT composition is not the same in the single-crystal region as that in the disordered region. Analyzing this effect is beyond the scope of the present work, and will be the object of another report. The microstructure of sample B (annealed at 420 °C, which corresponds to region 2 in Fig. 1(c)) is comparable to that of sample A, except that the oxidation front extents to approximately 40 nm in the GaAs substrate, and that the thickness of single-crystal PZT has doubled to 20 nm as compared to sample A. Most of the PZT is disordered in this sample, suggesting that complete PZT crystal ordering cannot by achieved by annealing under air. The reasons for this are elucidated in the following discussion.

The HAADF-STEM view of sample C (Fig. 2(c)) shows that annealing at 510 °C (region 3 in Fig. 1(c)) causes a significant deterioration of the heterostructure. The oxidation front extents to more than 400 nm in the GaAs substrate, and holes are detected in the oxidized regions of the substrate, suggesting significant porosification of the semiconductor.

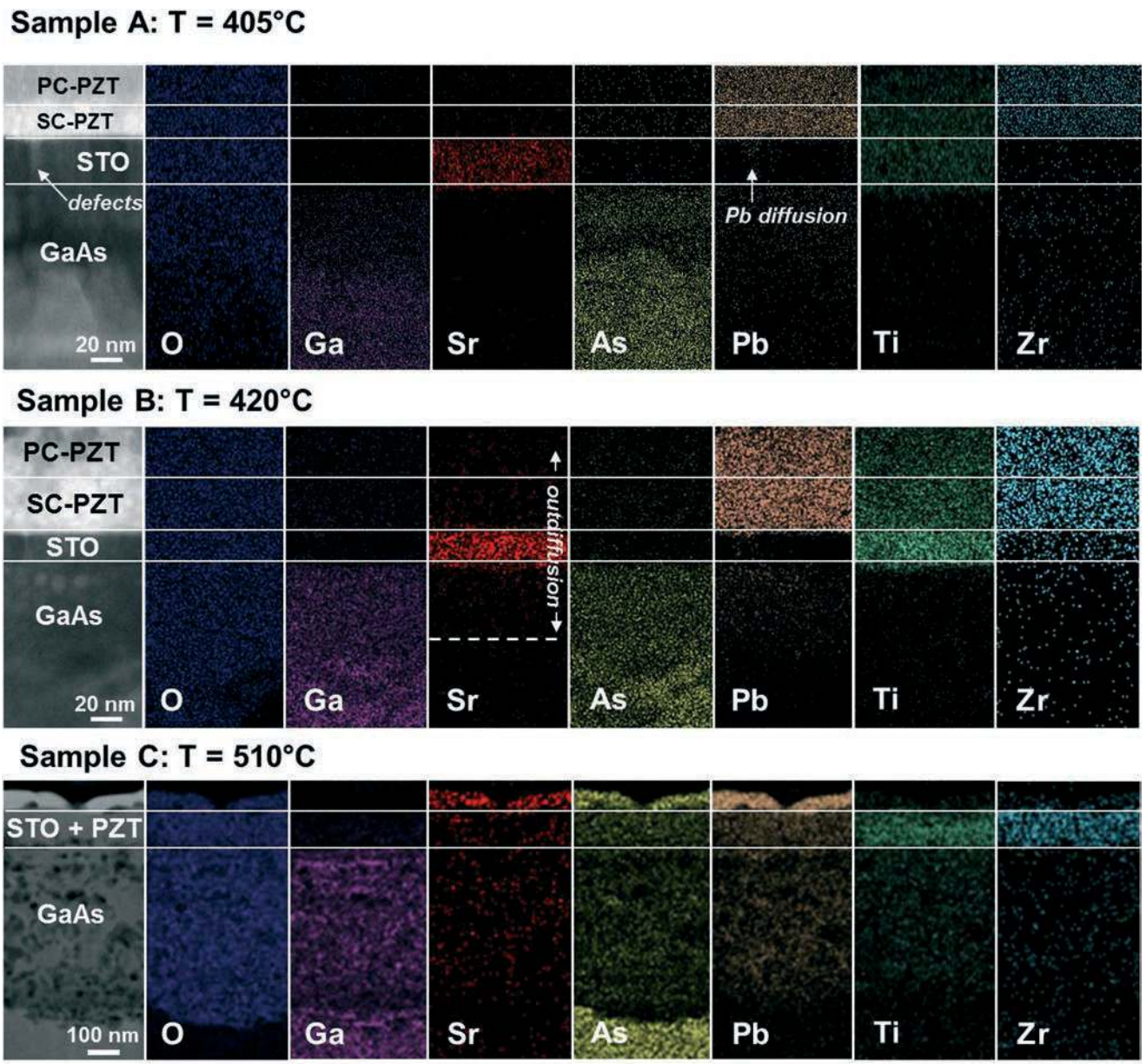

Fig. 3 EDX mappings of samples A, B and C, annealed at 405 °C, 420 °C and 510 °C, respectively. sc-(pc-)PZT stands for single-crystal (polycrystalline) PZT.

The interfaces between the different layers making up the heterostructure can only barely be distinguished, indicating strong intermixing across the entire structure. In the end, large islands are detected at the sample surface, caused by important segregation effects. EDX mappings of samples A, B and C presented in Fig. 3 provide further insights into the process leading to sample degradation during annealing.

The EDX mappings of sample A confirm the analysis of the HAADF-STEM image presented above: the interfaces between the different layers of the structure are rather abrupt, and oxygen significantly diffuses into the substrate. Interestingly, a significant amount of Pb is detected in the GaAs substrate underneath the oxide/GaAs interface, suggesting that Pb also diffuses from the PZT layer towards the substrate though the STO template. The vertical defect pointed out in the TEM image of sample A acts as a diffusion channel for Pb, as shown by the Pb mapping (detection of Pb in the STO layer, in the defect region). A similar phenomenon of cation diffusion enhancement in defective STO regions has already been reported, for instance in ref. 25.

Signatures for O and Pb diffusion towards the substrate are clearly detected in the EDX mappings of sample B. At this temperature, Sr also starts to diffuse towards both the GaAs substrate and the PZT film. This Sr out-diffusion is the cause of the degradation of STO crystallinity and related decrease of the diffraction intensity detected in this temperature range (region 2 in the Arrhenius plot of Fig. 1(c)).

EDX mappings recorded on sample C, annealed at 510 °C, confirm the deteriorated condition of this sample. The GaAs substrate is massively oxidized, and the oxidized region is also strongly depleted in As, suggesting that As oxides have evaporated from the substrate. Hence, As oxides are known as unstable and highly volatile.[26] The STO and PZT films are completely intermixed and form a single layer (the PZT/STO interface can no longer be distinguished) mainly composed of Zr and Ti. Pb Sr as well as As and O are not only homogeneously spread into the former STO and PZT layers but also into the oxidized GaAs region. In the end, the large islands at the sample surface are mostly composed of Pb, Sr, As and O. The PZT layer, rather undamaged in sample B, is strongly deteriorated in sample C due to intermixing effects which is consistent with the decrease of the PZT (002) reflection intensity in region 3 (Fig. 1(c)).

A more quantitative and accurate assessment of the intermixing phenomena described above is provided by the analysis of the quantitative EDX line scans displayed in Fig. 4.

Oxidation of the GaAs substrate appears clearly from these profiles. The oxidized GaAs regions in samples A and B are mostly composed of a mixture of Ga_2O_3 and As_2O_3 (60% O, 20% As and 20% Ga). A significant fraction of As oxide has evaporated from the substrate in sample C, where the former GaAs region mostly contains Ga and O in GaO_2 proportions. A closer look at the STO/GaAs interface in samples A and B allows for confirming that Sr diffuses out of the STO layer towards GaAs, and that GaAs also contains a significant amount of Pb. In sample B, As also diffuses out of the substrate towards the STO layer. In the end, As is present in a significant concentration across the entire stack of sample C, showing that As oxide evaporation from the substrate is "captured" by oxide layers.

The analysis presented here clarifies the mechanisms of structural and chemical degradation occurring during crystallization of sol–gel PZT deposited on STO templated GaAs substrates. First, the chemical affinity between As and Sr as well as between As and Pb promotes diffusion and intermixing phenomena: Pb is detected in GaAs even in a moderate temperature range (region 1), and Sr/As intermixing is also detected in this region. These effects do not significantly affect PZT crystallization in region 1, but lead to progressive degradation of the STO template and associated slowdown of PZT crystallization in region 2. In parallel, significant oxidation of the GaAs substrate is observed, since annealing is

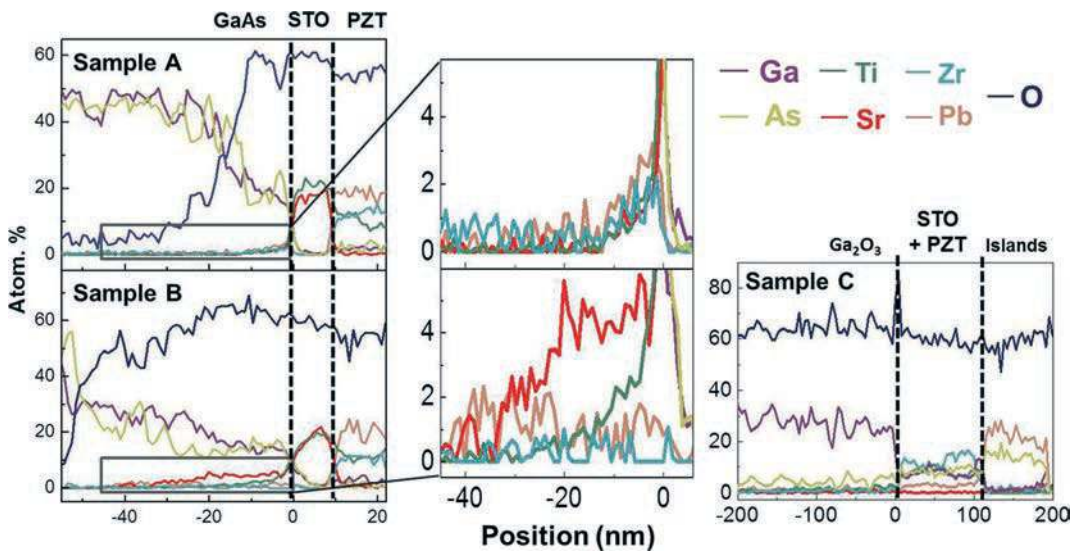

Fig. 4 Quantitative EDX profiles recorded on samples A, B, and C across the red dashed lines of Fig. 2.

carried out under air. This oxidation destabilizes As since As oxides are volatile, and the GaAs region is strongly depleted in As in the high temperature range (region 3). As destabilization promotes Sr/As intermixing and Pb diffusion towards the substrate. More critically, As oxides diffusing out of the substrate react with Pb and Sr across the entire structure (as indicated by the strong correlation between detection of As and detection of Pb and Sr in the EDX line scans), causing the major degradation of the stack in regime 3. In particular, Pb and Sr are spread over the entire structure and are present wherever oxidized As is detected, and desorbing As oxides bring Pb and Sr atoms up to the sample surface to form large islands composed of Sr, Pb, As and O. Of course, these chemical reactions affect the PZT crystallization process: degradation of the STO template in regime 2 hinders PZT crystallization, and the chemical integrity of the PZT layer is lost in regime 3.

Conclusion

As a conclusion, we have shown that the standard sol–gel process cannot be used to fabricate single-crystal PZT layers on STO templated GaAs substrates due to severe substrate oxidation, volatility of As oxides and strong chemical affinity between As anions and Sr and Pb cations. This illustrates that the chemical reactivity between the growing layer and the substrate may represent severe limitation for the integration of functional oxides on the GaAs platform, in particular if the sol–gel process requiring annealing in air environment for oxide crystallization has to be used. Nevertheless, solutions can be developed to circumvent this difficulty. First, a trade-off can be found regarding annealing: reduction of the annealing temperature and increase of the annealing duration, and/or reduction of the oxygen partial pressure may help in preserving the semiconductor integrity. Another solution consists of inserting a buffer layer of AlAs between the quantum well and the GaAs surface. The strong affinity between Al and oxygen should prevent the oxygen from diffusing to the inner III–V heterostructure. Preliminary tests of this solution have led to encouraging results that will be the object of another report.

Acknowledgements

This work was supported by the French Rhône-Alpes region, ARC6 project #14-010761-01. We acknowledge Agence Nationale de la Recherche (ANR), program of investment for the future, TEMPOS project (no. ANR-10-EQPX-50), for having funded the acquisition of the NANOTEM platform (Dual-beam FIB-FEG FEI SCIOS system and TEM-STEM FEI Titan Themis) used in this work.

References

1 K. Mistry, *et al.*, a 45 nm Logic Technology with High-k +Metal Gate Transistors, Strained Silicon, 9 Cu Interconnect Layers, 193 nm Dry Patterning, and 100% Pb-free Packaging, *Tech. Dig. - Int. Electron Devices Meet.*, 2007, 247–250.

2 S. B. Ogale, *Thin Films and Heterostructures for Oxides Electronics*, Springer, New York, 2005.

3 R. A. McKee, F. J. Walker and M. F. Chisholm, Crystalline Oxides on Silicon: The First Five Monolayer, *Phys. Rev. Lett.*, 1998, **81**, 3014.

4 R. A. McKee, F. J. Walker and M. F. Chisholm, Physical structure and inversion charge at a semiconductor interface with a crystalline oxide, *Science*, 2001, **293**, 468.

5 R. Droopad, Z. Yu, J. Ramdani, L. Hilt, J. Curless, C. Overgaard, J. L. Edwards, J. Finder, K. Eisenbeiser, J. Wang, V. Kaushik, B.-Y. Nguyen and B. Ooms, Epitaxial oxides on silicon grown by molecular beam epitaxy, *J. Cryst. Growth*, 2001, **227–228**, 936.

6 V. Vaithyanathan, J. Lettieri, W. Tian, A. Sharan, A. Vasudevarao, Y. L. Li, A. Kochhar, H. Ma, J. Levy, P. Zschack, J. C. Woicik, L. Q. Chen, V. Gopalan and D. G. Schlom, c-axis oriented epitaxial $BaTiO_3$ films on (001) Si, *J. Appl. Phys.*, 2006, **100**, 024108.

7 G. Niu, S. Yin, G. Saint-Girons, B. Gautier, P. Lecoeur, V. Pillard, G. Hollinger and B. Vilquin, Growth temperature dependence of epitaxial Gd_2O_3 films on Si(1 1 1), *Microelectron. Eng.*, 2011, **88**, 1232.

8 S. Abel, M. Sousa, C. Rossel, D. Caime, M. D. Rossell, R. Emi, J. Fompeyrine and C. Marchiori, Controlling tetragonality and crystalline orientation in $BaTiO_3$ nanolayers grown on Si, *Nanotechnology*, 2013, **24**, 285701.

9 C. Dubourdieu, J. Bruley, T. M. Arruda, A. Posadas, J. Jordan-Sweet, M. M. Frank, E. Cartier, D. J. Frank, S. V. Kalinin, A. A. Demkov and V. Narayanan, Switching of ferroelectric polarization in epitaxial $BaTiO_3$ films on silicon without a conducting bottom electrode, *Nat. Nanotechnol.*, 2013, **8**, 748.

10 S. Baek, J. Park, D. Kim, V. Aksyuk, R. Das, S. Bu, D. Felker, J. Lettieri, V. Vaithyanathan, S. Bharadwaja, N. Bassiri-Gharb, Y. Chen, H. Sun, C. Folkman, H. Jang, D. Kreft, S. Streiffer, R. Ramesh, X. Pan, S. Trolier-McKinstry, D. Schlom, M. Rzchowski, R. Blick and C. Eom, Giant Piezoelectricity on Si for Hyperactive MEMS, *Science*, 2011, **334**, 958.

11 Y. Liang, J. Kulik, T. C. Eschrich, R. Droopad, Z. Yu and P. Maniar, Hetero-epitaxy of perovskite oxides on GaAs(001) by molecular beam epitaxy, *Appl. Phys. Lett.*, 2004, **85**, 1217.

12 W. Huang, Z. P. Wu and J. H. Hao, Electrical properties of ferroelectric BaTiO3 thin film on SrTiO3 buffered GaAs by laser molecular beam epitaxy, *Appl. Phys. Lett.*, 2009, **94**, 032905.

13 R. Contreras-Guerrero, J. P. Veazey, J. Levy and R. Droopad, Properties of epitaxial $BaTiO_3$ deposited on GaAs, *Appl. Phys. Lett.*, 2013, **102**, 012907.

14 R. Ramesh, S. Aggarwal and O. Ociello, Science and technology of ferroelectric films and heterostructures for non-volatile ferroelectric memories, *Mater. Sci. Eng., R*, 2001, **32**, 191.

15 L. Louahadj, D. Le Bourdais, L. Largeau, G. Agnus, L. Mazet, R. Bachelet, P. Regreny, D. Albertini, V. Pillard, C. Dubourdieu, B. Gautier, P. Lecoeur and G. Saint-Girons,

Ferroelectric Pb(Zr,Ti)O_3 epitaxial layers on GaAs, *Appl. Phys. Lett.*, 2013, **103**, 212901.

16 W. Gong, J.-F. Li, X. Chu, Z. Gui and L. Li, Single-crystal Nb-doped Pb(Zr,Ti)O3 thin films on Nb-doped SrTiO3 wafers with different orientations, *Appl. Phys. Lett.*, 2014, **85**(17), 3818.

17 X. Meng, J. Cheng, B. Li, S. Guo, H. Ye and J. Chu, Low-temperature preparation of highly (1 1 1) oriented PZT thin films by a modified sol–gel technique, *J. Cryst. Growth*, 2000, **208**(1–4), 541.

18 S. Yin, G. Niu, B. Vilquin, B. Gautier, G. L. Rhun, E. Defay and Y. Robach, Epitaxial growth and electrical measurement of single crystalline Pb($Zr_{0.52}Ti_{0.48}$)O_3 thin film on Si(001) for micro-electromechanical systems, *Thin Solid Films*, 2012, **520**, 4595.

19 R. Moalla, B. Vilquin, G. Saint-Girons, G. Sebald, N. Baboux and R. Bachelet, Dramatic effect of thermal expansion mismatch on the structural, dielectric, ferroelectric and pyroelectric properties of low-cost epitaxial PZT films on $SrTiO_3$ and Si, *CrystEngComm*, 2016, **18**, 1887.

20 J. Gatabi, K. Lyon, S. Rahman, M. Caro, J. Rojas-Ramirez, J. Cott-Garcia, R. Droopad and B. Lee, Functional materials integrated on III-V semiconductors, *Microelectron. Eng.*, 2015, **147**, 117.

21 B. Meunier, R. Bachelet, G. Grenet, C. Botella, P. Regreny, L. Largeau, J. Penuelas and G. Saint-Girons, The role of Titanium at the $SrTiO_3$/GaAs epitaxial interface, *J. Cryst. Growth*, 2016, **433**, 139–142.

22 B. Meunier, L. Largeau, P. Regreny, R. Bachelet, B. Vilquin, J. Penuelas and G. Saint-Girons, Sol–gel deposition of Pb(Zr,Ti)O_3 on GaAs/InGaAs quantum well heterostructure via $SrTiO_3$ templates: Stability of the semiconductor during the oxide growth, *Thin Solid Films*, 2016, DOI: 10.1016/j.tsf.2016.01.037.

23 Z. Huang, Q. Zhang and R. W. Whatmore, Structural development in the early stage of annealing of sol–gel prepared lead zirconate titanate thin films, *J. Appl. Phys.*, 1999, **86**, 1992.

24 Y. Z. Chen, J. Ma and J. X. Zhang, Thermal analysis of the seeded lead zirconate titanate sol–gel system, *Mater. Lett.*, 2003, **57**, 3392.

25 W. H. Rhodes and W. D. Kingery, Dislocation Dependence of Cationic Diffusion in $SrTiO_3$, *J. Am. Ceram. Soc.*, 1966, **49**, 521.

26 C. W. Wilmsen, R. W. Kee and K. M. Geib, Initial oxidation and oxide/semiconductor interface formation on GaAs, *J. Vac. Sci. Technol.*, 1979, **16**, 1434.